DOI: 10.13009/EUCASS2019-181

DOI: ADD DOINUMBER HERE

Influence of Radial Stratification on Eigenfrequency Computations in Rocket Combustion Chambers

A. Chemnitz[⋆†] *and T. Sattelmayer*[⋆]
[⋆]*Chair of Thermodynamics, Technical University of Munich*
Boltzmannstr. 15, 85747 Garching, Germany
chemnitz@td.mw.tum.de
[†]Corresponding author

Abstract

The impact of a radially stratified mean flow on the flow field fluctuations in a rocket combustion chamber is studied using the Linearized Euler Equations. With the Finite Element Method eigenmodes are calculated for different degrees of stratification. Thereto a simplified diffusion flame structure is imposed via an analytic ansatz function. The complex eigenfrequencies are evaluated and the mode shapes are analyzed. Both eigenfrequencies and damping rates are found to decrease with increasing stratification. The mode shapes show a significant dependence on the stratification regarding vorticity and entropy fluctuations, whereas the pressure amplitudes are not influenced.

1. Introduction

Combustion instabilities are a critical aspect in the design of rocket combustion chambers. A coupling of heat release and pressure fluctuations potentially results in increased thermal and mechanical loads up to engine failure.[11] To identify thermoacoustic instabilities in early development stages, cost-efficient procedures are required that allow for the quick assessment of various designs. For this purpose, a hybrid simulation approach has been developed, which provided promising results in previous studies.[9,10] It is based on an eigensolution study of the Linearized Euler Equations (LEE) in frequency space. One simplification that allows for efficient calculations is the assumption of a quasi one-dimensional mean flow in the chamber, with mostly no gradients in radial direction. In the present study, the consequences of this simplification are addressed from a numerical point of view. Several mean flows that are equivalent when subjected to the averaging procedure which is used to obtain the quasi one-dimensional case are analyzed. Thereby, the degree of stratification, i.e. the maximum deviation from the radial mean is systematically varied. The studied configuration is based on the combustion chamber D (BKD) of the German Aerospace Center (DLR), see e.g. [5].

The radial stratification in rocket combustion chambers is a result of the presence of multiple diffusion flames. The fuel and oxidizer injectors are typical arranged coaxially with the combustion zone forming in the shear layer between the two jets. The induced gradients can impact the system stability in different ways. On the one hand the flame response is subject to the mixing processes in the shear layer. In this context e.g. the role of density gradients has been studied experimentally in [4]. On the other hand, the linear perturbation solutions for the chamber's eigenmodes take into account the spatial mean flow distribution, which therefore can impact the damping of the eigensolutions aside from any flame feedback. The current study focuses on the damping rates obtained for the mean flow and does not explicitly consider any flame dynamics. Besides the general importance of the mode damping related to the mean flow distribution, in the framework of the aforementioned hybrid approach the simplification of a quasi one-dimensional flow does not concern the flame response calculations.

Previous studies revealed that for a quasi one-dimensional mean flow a substantial amount of damping was present in the chamber,[9] which has been termed field damping and is related to the axial mean flow gradients. So there is an indication that dominant damping mechanisms are already captured without accounting for radial stratification. This contrasts the situation in gas turbine combustors, where shear layer induced vortex shedding has been identified to be of major importance for the damping rate determination.[6] In the current study, shear layers are now introduced via the radial stratification approach into the rocket engine calculations as well, allowing for a more explicit assessment of

DOI: 10.13009/EUCASS2019-181

the role of the different damping mechanisms.

In general, compressible flow is composed of acoustic, vorticity and entropy contributions,[1] which occur as separate modes in a linear eigensolution analysis.[3] The acoustic part is closely related to the analytical solution of uniform cylindrical duct flows. For rocket engine combustion instability, the modes of transverse type (T_{nT}, n_T denoting the tangential mode order) are generally of highest relevance. While a discussion of duct flow acoustics in the context of rocket combustion chambers can be found e.g. in [9], here only a key property, which is relevant for the interpretation of the results is recapitulated. The cut-on frequency is calculated as

$$\omega_{co} = \frac{s_{n_T n_R} c}{r_c} \sqrt{1 - Ma^2} \tag{1}$$

with the sound speed c, the chamber radius r_c and the Mach number Ma. $s_{n_T n_R}$ denotes the $n_R{}^{\text{th}}$ root of the derivative of the $n_T{}^{\text{th}}$ Bessel function, where n_R is the radial order of the mode. A transverse mode can only persist at frequencies above the cut-on frequency. Below, it exponentially decays in axial direction. This has been previously found to strongly influence the amplitude distributions for transverse modes and will be of relevance for the discussion in section 4.

In the following sections, the numerical setup used in this study is described; The procedure to obtain the mean-flows is outlined, followed by the discussion of the simulation results and the conclusions.

2. Numerical Setup

The numerical approach consists of three sequential steps: the simulation of a single flame, the calculation of the mean flow based on the single flame results and finally the perturbation simulation for the determination of the stability behavior. In this section, an overview of the single flame and the perturbation simulation is given. Due to its significance in the present study, the step of the mean flow calculation is discussed in a subsequent, separate section.

2.1 Perturbation Simulations

The perturbation simulations are based on an eigenvalue analysis using a stabilized Finite Element approach. In the following, the governing equations are outlined, then the boundary conditions are given and the grid design is discussed together with the numeric stabilization.

2.1.1 Governing Equations

The perturbation computations are carried out in frequency space. Thereto, the fluctuation ϕ' of a quantity $\phi = \overline{\phi} + \phi'$ is expressed as harmonic oscillation in terms of its complex amplitude $\hat{\phi}$, the angular frequency $\omega = 2\pi f$ and the damping rate α:

$$\phi' = \Re\mathfrak{e}\left[\hat{\phi}\exp\left(i\Omega t\right)\right] = \Re\mathfrak{e}\left[\hat{\phi}\exp\left((i\omega - \alpha)t\right)\right] \tag{2}$$

with Ω denoting the complex eigenfrequency. In the following, the term eigenfrequency is used to refer to the real valued eigenfrequency, if not explicitly stated otherwise. To further reduce the computational effort, the simulation domain is modeled as two-dimensional. Thereto, a cylindrical coordinate system (r, θ, x) is used with the azimuthal dependence being described via the analytic solution for circular duct flow acoustics, following [7]:

$$\hat{\phi} = \tilde{\phi}\exp\left(in_T\theta\right) \quad . \tag{3}$$

The transverse order of the studied mode, n_T, is thereby defined before the simulation is conducted.

The above modeling approaches are used to simplify the Linearized Euler Equations, which are formulated as mass

$$i\Omega\hat{\rho} + \hat{\boldsymbol{u}}\cdot\nabla\overline{\rho} + \hat{\rho}\nabla\cdot\overline{\boldsymbol{u}} = 0 \quad , \tag{4}$$

momentum

$$i\Omega\hat{\boldsymbol{u}} + \left(\hat{\boldsymbol{u}}\cdot\nabla\right)\overline{\boldsymbol{u}} + \left(\overline{\boldsymbol{u}}\cdot\nabla\right)\hat{\boldsymbol{u}} + \frac{1}{\overline{\rho}}\nabla\hat{p} - \frac{\hat{\rho}}{\overline{\rho}^2}\nabla p = 0 \tag{5}$$

DOI: 10.13009/EUCASS2019-181

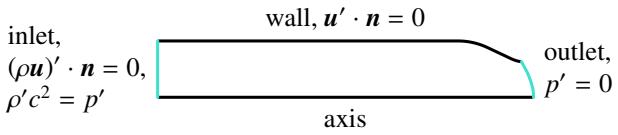

Figure 1: Boundary conditions

and pressure equation

$$i\Omega\hat{p} + \overline{\boldsymbol{u}} \cdot \nabla\hat{p} + \hat{\boldsymbol{u}} \cdot \nabla\overline{p} + \kappa(\overline{p}\nabla \cdot \hat{\boldsymbol{u}} + \hat{p}\nabla \cdot \overline{\boldsymbol{u}}) - \frac{1}{\kappa - 1}(\hat{\boldsymbol{u}}\overline{p} + \overline{\boldsymbol{u}}\hat{p}) \cdot \nabla\kappa = 0 \quad . \tag{6}$$

Here u denotes the velocity, ρ the density, p the pressure and κ the isentropic compressibility. The usage of the anisentropic set of equations despite the lack of flame feedback is necessary since the strong flow gradients potentially induce entropy fluctuations as can be seen from the source term formulation[8] of the LEE.

2.1.2 Mesh and Boundary Conditions

The simulation covers the whole subsonic region of the combustion chamber, including parts of the nozzle. The geometry of the domain is shown in Fig. 1. The nozzle is modeled up to the supersonic region, where it ends shortly behind the sonic line. That way the acoustic boundary of the subsonic chamber part at Mach 1 is captured while supersonic processes are mostly excluded from the calculations. The other boundary conditions are summarized in Fig. 1. The inlet is modeled uniformly in radial direction. It is considered to be neutral in terms of acoustic energy by setting the mass flow fluctuations to zero. Entropy fluctuations are convectively transported and directly depend on the calculated pressure and density perturbations. To ensure that the solution only contains entropy fluctuations generated inside the domain, an isentropic relation between pressure and density is enforced at the inlet. The wall is modeled as acoustically hard. Due to the supersonic outflow, the outlet boundary condition is of minor importance, however, zero pressure fluctuations have been found to be advantageous for the numeric stability of the solution.

The LEE are discretized on the domain using linear finite elements. A common grid is designed that provides satisfactory results for all cases. To this end, the case with the maximum gradients and therefore highest sensitivity to the element size is considered first. As the damping rates are significantly more grid-dependent than the eigenfrequencies, they are selected to judge the grid convergence. The front quarter of the chamber has been found to be of highest relevance regarding the grid resolution. It is refined by a factor of four compared to the rear chamber section with a smooth transition in between. Since the discretization induces numerical instabilities in the solution,[2] a stabilization term is added to the weak form.[2,9] The strength of stabilization is controlled via the parameter τ_s. Fig. 2(a) shows the damping rate in dependence of the element number n_{el} and the stabilization parameter. The spatial refinement of the grid is performed equally for both dimensions and two orders of magnitude are covered regarding the number of cells. After strong fluctuations at low resolutions, convergence of the damping rate is observed for finer grids. The configuration with about $n_{el} = 4.4 \cdot 10^5$ elements is selected for the computations in the present study. For this grid the higher resolved development of the damping rate via the stabilization parameter is shown for three different stratification amplitudes in Fig. 2(b). The region of possible values for the stabilization is bounded above by the occurrence of numerical artifacts in the solution. These manifest as regions of unreasonably high amplitudes, emanating from the chamber outlet close to the axis. Here, the limiting value is about $\tau_s \approx 0.2$. Based on a comparison of certain amplitude distributions with characteristic properties to be satisfied by the correct solution, a value of $\tau_s = 0.07$ is selected for the stabilization parameter.

2.2 Single Flame Simulations

The single flame simulations provide the axial distributions of heat release, sound speed and isentropic compressibility that are used for the calculation of the mean flow. As the profiles for the current study are approximations to those derived from a single flame solution, its setup is outlined briefly. The calculations are carried out as finite volume simulation with ANSYS® Fluent 18.0. The stationary Reynolds Averaged Navier Stokes Equations are solved on a two-dimensional axis-symmetric domain with the k-ε model for turbulence closure. Combustion is modeled via a semi-diabatic flamelet approach, i.e. the flow composition is obtained from adiabatic calculations while the temperature is adapted according to the local enthalpy. To capture the fluid behavior at the low injection temperatures, the

DOI: 10.13009/EUCASS2019-181

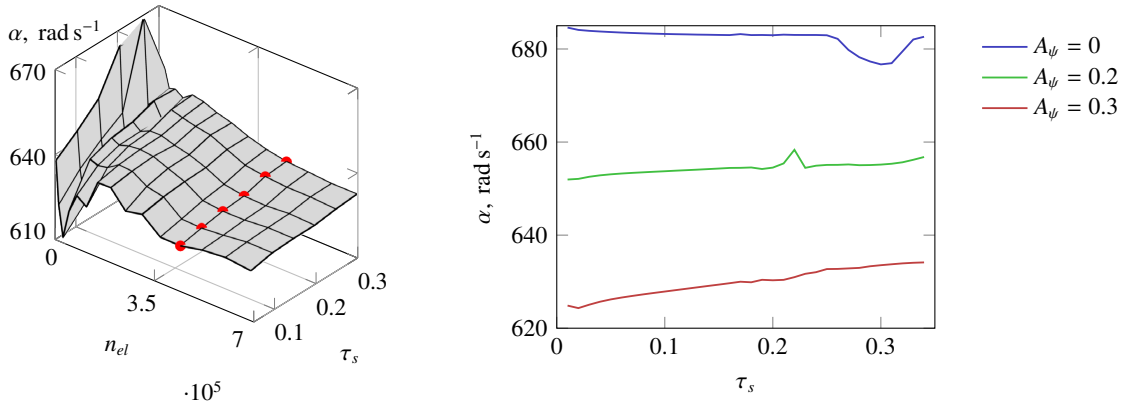

(a) resolution and stabilization; red: final grid

(b) stabilization

Figure 2: Grid and stabilization sensitivity

Soave-Redlich-Kwong real gas equation of state is used.

3. Mean Flow Calculation

The mean flow is the linearization state for the LEE. Its calculation procedure is designed to reproduce, on area weighted radial average, those quantities of the single flame simulation that characterize its acoustics. To ensure consistency with the assumptions involved in the derivation of the LEE, the mean flow is obtained as solution of the Euler Equations. Thereby clearly defined source terms combined with the local adaption of the flow properties are used to model specific flow features. In the following, the basic procedure that is used to obtain the quasi one-dimensional flow is described, providing the basis for the subsequent introduction of the stratification into the mean flow.

3.1 Quasi One-Dimensional Flow

The methodology presented in this section is an enhanced version of the one used in [9, 10] to obtain the mean flow for the rocket engine stability analysis. It ensures that the Euler Equations are fulfilled by the mean flow to such a degree as they are represented in the LEE: pressure, density and velocity are calculated as solution of the Euler Equations, with the gas constant R and the isentropic coefficient κ being determined from the desired axial distributions of sound speed and isentropic compressibility as described below. These are extracted from the single flame simulations via radial area weighted averaging (subscript $1D$). The heat release due to combustion is represented via a one-dimensional energy source term, again based on the single flame simulations. The flow is injected uniformly across the domain inlet (cf. Fig. 1), the wall is of no-slip type and the outflow through the nozzle exit is supersonic. As a result of this approach, significant two-dimensional structures are only present in the nozzle region, while the flow in the cylindrical chamber section remains one-dimensional.

When R is given, κ determines the specific isobaric heat capacity c_p. However, c_p influences the solution only via a temperature integral. Conclusively, its isolated value at the solution temperature can be adapted arbitrarily during post-processing without influencing the fact that the fields are consistent with the Euler Equations. This is used to ensure that the most important quantity for acoustic simulations, the sound speed, is reproduced by the mean flow:

$$\kappa = \frac{\rho}{p} c^2 \quad . \tag{7}$$

So the remaining parameter to be determined is the gas constant. Unlike the isentropic coefficient it needs to be adapted during the simulation to ensure the outcome to be a valid solution of the Euler Equations and the ideal gas equation of state. The gas constant is calculated in such a way that at the correct sound speed, the axial profile of

DOI: 10.13009/EUCASS2019-181

isentropic compressibility η is matched. Thereto, a target density

$$\rho_{1D} = \frac{1}{\eta_{1D} c_{1D}^2} \tag{8}$$

is calculated and the gas constant is obtained during the simulation from the ideal gas law

$$R = \frac{p}{\rho_{1D} T} \tag{9}$$

with T denoting the temperature. That way, the solution possesses the correct density to match the averaged isentropic compressibility and is consistent with the ideal gas equation of state.

3.2 Stratified Flow

The basic procedure for the calculation of the stratified flow corresponds to the quasi one-dimensional approach. However, instead of prescribing one-dimensional profiles, two-dimensional reference distributions are used for sound speed and density. These are obtained by applying a stratification function ψ to the respective one-dimensional profiles. Like for the one-dimensional case, the inlet is considered as a single boundary, i.e. no injectors are resolved. However, a radial profile is imposed on the inlet temperature that is consistent with the stratification of the sound speed (cf. Eq. 15). Since the Euler Equations do not include cross-stream transport effects, the homogenization of the flow fields in the rear part of the chamber needs to be modeled explicitly as well. This is done by defining an axial dependence of the stratification that goes from maximum at the inlet to zero as the flow passes through the chamber. The energy source is derived to be consistent with this behavior. With these prerequisites again the Euler Equations are solved to obtain the mean flow field.

The acoustic key parameter for the mean flow is the distribution of the sound speed. So this quantity is the starting point for the design of the flow stratification. Its target value is calculated as

$$c_{ref} = c_{1D} \psi \tag{10}$$

with the stratification function ψ ensuring the correct reproduction of the radial area weighted mean, i.e.

$$\frac{1}{\pi r_c^2} \int_0^{r_c} c_{ref} 2\pi r dr = c_{1D} \quad . \tag{11}$$

The stratification function is specified via the stratification amplitude A_ψ, the radial shape function ψ_x and the radial stratification function ψ_r as

$$\psi = 1 + A_\psi \psi_x \psi_r \quad . \tag{12}$$

The profile shall be sufficiently smooth to ensure good numeric solvability. As can be seen from the single flame solution shown in Fig. 3, the sound speed is higher in the outer flame regions and lower in the cold oxidizer core. Thus, for the radial stratification a cosine distribution is chosen:

$$\psi_r = cos(2\pi \frac{r}{r_c} n_{fl}) \tag{13}$$

with the chamber radius r_c and the number of flame structures in radial direction n_{fl}. In the present study a configuration with two flame structures is considered. As the flow moves downstream, turbulent mixing causes the flame to close at the axis and leads to a homogenization. This is modeled via the axial shape function

$$\psi_x = \begin{cases} 1, & x \leq x_s \\ 0.5 + 0.5 \cos\left(\pi \frac{x - x_s}{x_f - x_s}\right), & x_s < x < x_f \\ 0, & x \geq x_f \end{cases} \quad . \tag{14}$$

with x_s the axial starting position of the homogenization process and x_f the end point. Note, that this function just governs the development of stratification, i.e. the underlying axial sound speed profile is still c_{1D} as extracted from the single flame simulation. From the sound speed distribution, approximate stratification functions for the heat source and density are derived, based on

$$T \propto c^2 \propto \psi^2 \quad . \tag{15}$$

DOI: 10.13009/EUCASS2019-181

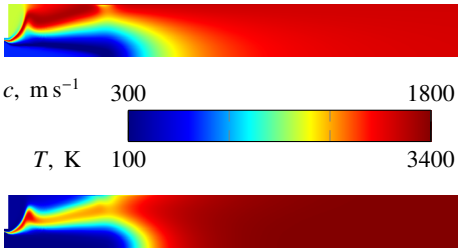

Figure 3: Single flame temperature distribution; axial dimension scaled by 0.25

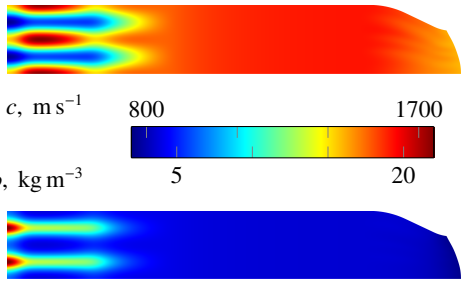

Figure 4: Mean flow fields at a stratification amplitude of $A_\psi = 0.3$

and

$$\rho \propto \frac{1}{T} \quad . \tag{16}$$

The radial stratification of temperature and thus density also induces shear layers in the mean velocity fields. To enhance the axial decrease of the velocity stratification, an additional momentum source term u is applied in the cylindrical part of the chamber:

$$\mathrm{u} \propto \frac{\dot{m}}{A} - \rho u \tag{17}$$

with the total mass flow $\dot{m}$ and the cylindrical chamber cross section A.

4. Results

The T_1 eigensolutions obtained with the previously described setup are discussed in this section. Beforehand, the obtained mean flow results are covered briefly. Then, the complex eigenfrequencies are considered. The mode shapes, i.e. the spatial distribution of the complex amplitudes of the solution fields are analyzed, taking into account the contributions of acoustic, vorticity and entropy perturbations.

4.1 Mean Flow

The stratified mean flow is the basis of the current study. Thus its structure as it results from the setup outlined in the previous section is addressed before continuing with the perturbation analysis. The first step of the mean flow generation is the single flame simulation. The resulting sound speed and temperature distribution are given in Fig. 3. While the sound speed distribution increases from the axis towards the outer domain boundary at it has been modeled in the stratification function, the temperature shows a decrease outside of the combustion zone located in the mixing layer. The differing behavior between these fields is caused by the varying flow composition, a property that is neglected in the artificial stratification approach. As can be seen in Fig. 4 the shape of the sound speed distribution is described appropriately by the stratification model of the mean flow. The upper limit is matched quite well, while the sound speed in the region of cold oxidizer is higher than in the single flame simulation. A detailed view of the sound speed profile is given in Fig. 5. The one-dimensional distribution that the field is based upon is shown along with the radial profile at the inlet for different stratification amplitudes. Regarding the density distribution (Fig. 4) the lower limit is approximated quite well by the stratification while the upper limit is found to lie below that of the single flame simulation. Again, the oxidizer cores are clearly visible.

4.2 Eigenfrequency and Damping

The real valued eigenfrequencies are shown in Fig. 6. With increasing stratification amplitude, the eigenfrequency decreases. Starting from the uniform case, initially a close to linear dependence on the stratification amplitude is observed. At higher stratification, the rate of frequency decrease increases. The overall variation in the considered stratification range is about 100 Hz, corresponding to a relative change of less than 1 %. A possible reason for the

DOI: 10.13009/EUCASS2019-181

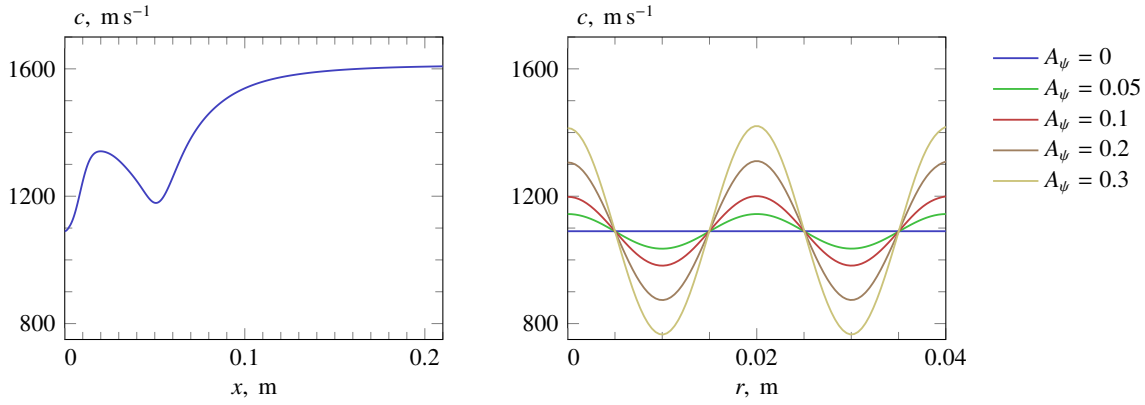

(a) axial 1D profile (b) inlet

Figure 5: Sound speed distribution

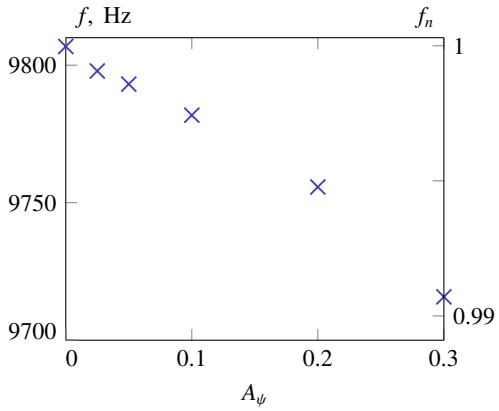

Figure 6: Eigenfrequencies via stratification amplitude

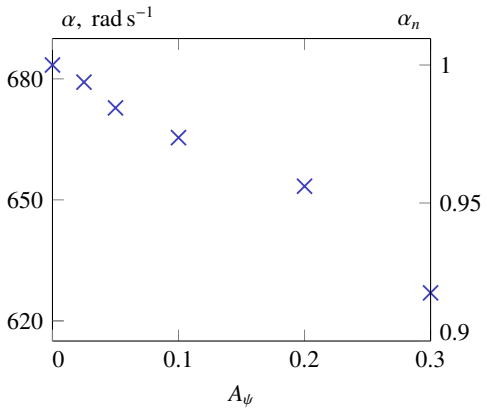

Figure 7: Damping rates via stratification amplitude

decreasing trend is the strong connection of the cut-on frequency and the T_1 frequency. For the cut-on frequency

$$f_{co} \propto c\sqrt{1 - Ma^2} \tag{18}$$

holds (cf. Eq. 1). Since in the stratified flow approach under the premise of a constant mass flux $u \propto \frac{1}{\rho} \propto T \propto c^2$ applies, it follows that $Ma = u/c \propto c$. Conclusively, if the last factor in Eq. 18 is considered as weighting factor, the flow stratification leads to regions of low sound speed to contribute more to the effective cut-on frequency than those of high sound speeds. With increasing stratification, there are also more distinct regions of lower sound speed, leading to a decrease of the effective cut-on frequency and thus the T_1 eigenfrequency of the chamber. Regarding the procedure for the mean flow calculation, this indicates that an equal radially averaged sound speed does not exactly ensure equal eigenfrequencies for transverse modes.

The damping rates as a function of stratification amplitude are given in Fig. 7. The overall level is rather high with more than 600 rad s^{-1}. This can be attributed to the aforementioned strong field damping found in rocket combustion chambers. Like for the eigenfrequencies, a decrease with increasing stratification amplitude is observed. While the absolute variation is about one order of magnitude smaller as for the eigenfrequency, the opposite is true for the relative change of the damping rate, which goes up to 10 % in the considered stratification amplitude range. The damping rate can be strongly affected by the interplay of the different mode contributions (acoustic, vortical and entropy). So it is in general not covered by the analytical approach used for the interpretation of the eigenfrequencies.

DOI: 10.13009/EUCASS2019-181

Figure 8: Pressure amplitude distribution

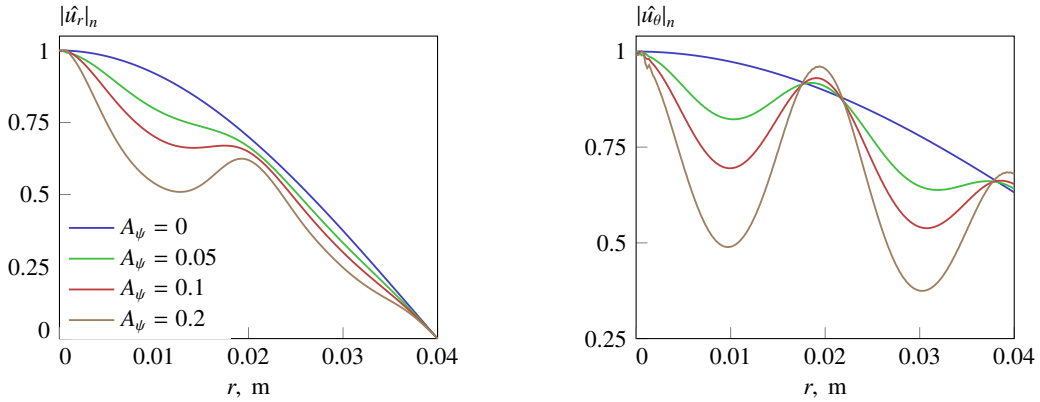

(a) radial velocity

(b) circumferential velocity

Figure 9: Velocity amplitudes at the inlet

4.3 Mode Shapes

The mode shape refers to the spatial distribution of the complex amplitudes of the different fluctuating fields. These can be considered to be a superposition of acoustic, entropy and vorticity fluctuations. The acoustic T_1 mode shape in rocket combustion chambers is strongly affected by the sound speed distribution resulting from the combustion. The high axial gradients of sound speed causes the cut-on frequency to vary accordingly. This leads to the T_1 mode to be cut on in the front region of the chamber first, while being still cut off in the rear part. The principal shape of the pressure amplitude distribution persists also in the presence of axial gradients. For the case without stratification it is shown in Fig. 8, in normalized form (subscript n). This mode shape is not affected by the degree of stratification, i.e. even at the maximum considered stratification amplitude of 0.3, there is no significant deviation from the distribution shown in Fig. 8.

While the pressure is dominated by the acoustic mode, density and velocity fluctuations are subject to influences of entropy and vortical perturbations. First, the velocity fluctuations (acoustic as well as vortical) are considered. The profiles of radial and circumferential velocity fluctuations are shown in Fig. 9. While the pressure fluctuations remain unchanged by the stratification, the radial mean flow profile manifests in the associated velocity fluctuations. For the flow stratification, the characteristic specific acoustic impedance

$$\rho c \propto \frac{c}{T} \propto \frac{1}{c} \tag{19}$$

is obtained, i.e. in regions of higher sound speed the velocity fluctuations increase. For the unstratified case the radial velocity fluctuations again correspond to the analytical profile whereas for stratified mean flow the two inner peaks in the sound speed distribution induce peaks in the amplitude profile (cf. Fig. 9(a)). However, since these are still superimposed with the overall T_1 mode shape, i.e. the radial velocity decaying to zero at the wall, the outer sound speed peak does not lead to a velocity amplitude peak. The circumferential velocity fluctuations are not affected by the wall boundary conditions. Here, all three sound speed peaks result in local maxima, as can be seen in Fig. 9(b).

Besides the just discussed influence of the acoustics on the velocity fluctuations, vortical perturbations occur. For different degrees of stratification, the circumferential component of the vorticity fluctuations is shown in Fig. 10. The fields are normalized with the respective maximum pressure amplitude for better comparability between the cases. For the uniform case vortical structures are already visible, that arise from the axial mean flow gradients. They are rather uniform across the chamber radius with only some influence of the wall boundary conditions in the outer region. The vorticity fluctuations arise from the axial flow gradients and are transported convectively, which leads to the increasing distance between adjacent peaks in the rear chamber section due to the increasing flow velocity. In the nozzle part,

DOI: 10.13009/EUCASS2019-181

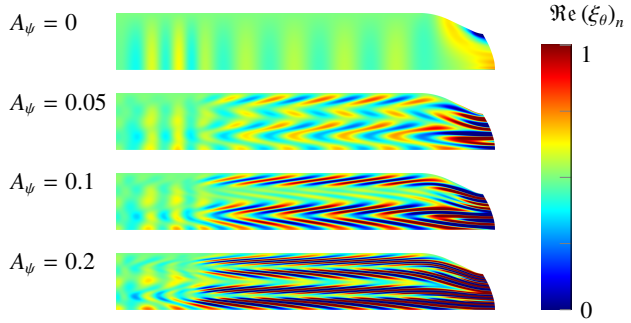

Figure 10: Real part of the circumferential vorticity amplitude

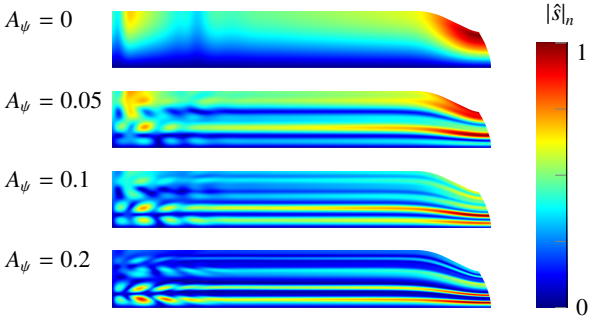

Figure 11: Entropy amplitude

the flow is redirected and accelerated, which leads to the production of additional vortical velocity fluctuations. Once stratification is involved, the shear layers associated with the flame structures exert a strong impact on the vorticity distribution. While in the front region the structures of the uniform case are still visible, the rear part of the chamber is dominated by vortices shed from the shear layers. The higher the stratification amplitude, the stronger the vorticity and the more the region close to the face plate is influenced by the vortical streets. Thereby the increase in strength is not equal across the chamber radius but some streets' intensity increases faster than others'. This can be linked to the cylindrical geometry as well as the transverse nature of the mode which already imposes radially non-uniform distributions of the fluctuating fields.

Finally, entropy fluctuations contribute to the eigenmodes. The respective amplitude distributions are shown in Fig. 11. Like the vorticity, entropy fluctuations are convected with the mean flow and produced even in the uniform case. The stratification imposes a dominant radial pattern across the whole chamber length. As has been observed for the vorticity, not all entropy streaks are equally sensitive towards the stratification amplitude. For low stratification the T_1 structure of the uniform flow is retained in the intensity of the different streaks. However, the entropy fluctuations close to the axis increase faster with increasing stratification and become dominant for higher stratification amplitudes. The structures observed for the entropy fluctuations are found to clearly appear in the distribution of the density amplitudes as well, particularly for cases with high stratification. Conclusively, entropy disturbances are of major importance for the mode shape.

5. Conclusions

An eigenmode analysis of a rocket combustion chamber has been conducted for different degrees of radial flow stratification. Based on a trigonometric ansatz function with varying amplitude values, mean flows fulfilling the Euler Equations and equal in radially averaged sound speed and isentropic compressibility have been calculated. For these mean flows, the first transverse eigensolutions of the LEE have been obtained.

The eigenfrequencies have been found to decrease with increasing stratification amplitude. A possible explanation has been found in the analytical cut-on frequency, which indicates a stronger weighting of regions with low sound speed for the effective cut-on frequency in the current setup. The relative deviation of the eigenfrequency however is small, staying below 1 %. The damping rate decrease with increasing stratification as well. Here, the sensitivity is higher with a maximum deviation of slightly below 10 % for the studied parameter range. Nevertheless, the fact that a high portion of the damping is already contained in the uniform mean flow indicates, that the stratification is not necessarily a dominant factor in the damping rate calculations. For the degrees of stratification covered in the present study, the axial mean flow gradients already capture relevant damping mechanisms. The identification of the reason for the decrease of the damping rate with increasing stratification needs further research.

The amplitude distributions of the fluctuating fields have been found to react differently to the stratification. The pressure distribution is uninfluenced by the stratification amplitude and only governed by the axial flow profile. However, the dependence of the characteristic acoustic impedance on the radial position induces a corresponding profile in the acoustically dominated parts of the velocity fields. Structures emanating from the shear layers have been found to dominate the vortical distributions in the rear section of the chamber, where they obscure the distribution resulting

DOI: 10.13009/EUCASS2019-181

from the axial flow gradients. Likewise the entropy amplitudes are affected by the stratification with the radial distribution depending on the stratification amplitude. For low stratification, the profile of the uniform case is reflected in the relative strength of the entropy streaks, whereas for high stratification the regions close to the chamber axis become dominant. The appearance of the structures observed for the entropy fluctuations in the density amplitude distributions shows the importance of entropy perturbations for the mode shape.

So while the eigenfrequencies are moderately affected by radial mean flow stratification, the mode shapes show a more pronounced and complex sensitivity towards the stratification. In continuation of the present study, further research will also cover the effect of the number of flame structures on the solution.

6. Acknowledgments

Financial support has been provided by the German Research Foundation (Deutsche Forschungsgemeinschaft – DFG) in the framework of the Sonderforschungsbereich Transregio 40.

References

[1] B. Chu and L.S.G. Kovasznay. Non Linear Interactions in a Viscous Heat-Conducting Compressible Gas, 1958.

[2] J. Donea and A. Huerta. *Finite Element Methods for Flow Problems*, chapter Stabilization Techniques, pages 59–65. John Wiley & Sons, Chichester, 2005.

[3] R. Ewert and W. Schröder. Acoustic Perturbation Equations Based on Flow Decomposition via Source filtering. *J. of Comp. Physics*, 188:365–398, 2003.

[4] A. Ghosh. *The Role of Density Gradient in Liquid Rocket Engine Combustion Instability*. PhD thesis, 11 2008.

[5] S. Gröning, D. Suslov, M. Oschwald, and T. Sattelmayer. Stability Behaviour of a Cylindrical Rocket Engine Combustion Chamber Operated with Liquid Hydrogen and Liquid Oxygen. In *5th European Conference for Aeronautics and Space Sciences EUCASS 2013*, 2013.

[6] T. Hofmeister, T. Hummel, B. Schuermans, and T. Sattelmayer. Modeling and Quantification of Acoustic Damping Induced by Vortex Shedding in Non-Compact Thermoacoustic Systems. In *Proceedings of the ASME Turbo Expo 2019: Turbomachinery Technical Conference and Exposition*, 2019.

[7] G. A. Mensah and J. P. Moeck. Efficient Computation of Thermoacoustic Modes in Annular Combustion Chambers Based on Bloch-Wave Theory. In *The American Society of Mechanical Engineers Turbo Expo 2015: Turbine Technical Conference and Exposition*, volume 4B: Combustion, Fuels and Emissions, June 2015. Paper GT2015-43476.

[8] C. Pankiewitz. *Hybrides Berechnungsverfahren für Thermoakustische Instabilitäten von Mehrbrennersystemen*. PhD thesis, Technische Universität München, 2004.

[9] M. Schulze. *Linear Stability Assessment of Cryogenic Rocket Engines*. PhD thesis, Technische Universität München, 2016.

[10] M. Schulze and T. Sattelmayer. Linear Stability Assessment of a Cryogenic Rocket Engine. *International Journal of Spray and Combustion Dynamics*, pages 1–22, May 2017.

[11] G. P. Sutton and O. Biblarz. *Rocket Propulsion Elements*. John Wiley & Sons, New York, 7th edition, 2001.